PROCESSING OF A MULTISCALE MULTIPHASE COMPOSITE

Hostettler, N.[1,2], Hubert, P.[1,2]*
[1] Structures and Composite Materials Laboratory, McGill University, Montréal, Canada
[2] Research Center for High Performance Polymer and Composite Systems
* Corresponding author (pascal.hubert@mcgill.ca)

Keywords: *Graphene, Multiphase, Manufacturing*

1 INTRODUCTION

Graphene enhanced composites are strong candidates to solve uncontrolled damage propagation in composites as they were found to increase the toughness and electrical conductivity of the matrix. The latter enabling sensing by continuous resistivity measurements, tracking the damage progression in the part [1]. When high quality graphene is too expensive for large part processing, more affordable graphene, produced at industrial volumes, would be needed in larger quantity to reach equivalent toughening and electrical properties increasing the risk of filtering effect and reaggregation during processing [2]. The increase in viscosity linked to the use of large quantity of graphene can be a challenge to the good impregnation of the fibre preform impacting the mechanical properties of the cured part. Blending the thermoset resin with a thermoplastic low-profile additive (LPA) in a control manner can create a self-assembly network of graphene and is a solution to shift the percolation threshold toward lower quantity of particles [3] [4]. However, the resulting increase of viscosity could lead to fibre infiltration issues. Furthermore, phase separations can be sensible to pressure and a bad control over the process could simply ruin the formation of a graphene network by shifting the critical point of phase separation toward lower quantity of thermoplastic [5]. In such a case, the critical concentration of graphene at the percolation threshold would increase, the graphene being trapped into isolated nodules of thermoset resin.
The objective of this research is to study the effect of the processing cycle on the impregnation of the fibre preform by an unsaturated polyester resin system produced by compression resin transfer moulding. The effect of fibres, pressure and graphene content on the phase separated morphology will be studied. The influence of the fibre architecture on the graphene filtration will be discussed. The final goal being to have an optimized processing cycle for a reliable production of quality multiscale multiphase composite plates.

2 MATERIALS AND METHODS

Preparation of the resin system

The resin system used in this research was the Polylite 31289, a pre-accelerated unsaturated polyester from *Reichhold* that was cured with 2wt% of Norox Azox from *United-initiator* ($t_{gel} = 3\text{min}$). The thermoplastic LPA was the CAPA 6500 from *Ingevity* a polycaprolactone (PCL) with a mean molecular weight of 50'000 g/mol. The graphene powder was the GrapheneBlack 3X from *NanoXplore inc.*, a mass-produced industrial graphene with a primary particle size between 1-2 µm and mean agglomerates size of D50 < 30 µm. The particles are between 6 to 10 graphene-layers thick with a carbon to oxygen ratio of 96:1 and a bulk density of 0.2 - 0.3 g/cm^3 [6]. Based on the

classification framework proposed by Bianco *et al.* [7], Wick *et al.* [8] and the ISO/TS 21356 – 1:2021, this graphene powder is classified as few-layer graphene nanoplatelets. The resin system was produced as follow: (i) the desired quantity of graphene was weighted and added to the neat resin, (ii) 1wt% of a mixture of Styrene/15wt% Triton X100 was added to the resin as a surfactant to help dispersing the graphene, (iii) the system was dispersed with a probe sonicator (*Hielscher* UP400St) for two cycles of 7min spaced by a 15min cool down step to limit the increase in temperature, (iv) the jar was then transferred into a 65°C preheated water bath where the desired quantity of PCL pellets was added and mixed for 20 min at 1500 rpm until fully dissolved, (v) the system was let to rest at room temperature for 20 min to stabilize the phase separated morphology, (vi) 2wt% of initiator was incorporated in the system before degassing for 1-2 min to be ready for processing.

Fibre and compression moulding

To understand the influence of the moulding parameters on the apparition of defects, several moulding cycles were tested on a bidirectional-glass-complex 0/90/Mat preform with a nominal superficial density of 910 g/m^2 from *SAERTEX.* To put in perspective the observations of the fibre architecture's effect on the filtering of graphene particles, other tests were performed on a twill weave from *Hexcel* with a nominal superficial density of 295 g/m^2. The details of the stacking configuration as well as the target thickness is shown in Table 1. The processing of the plates was conducted by compression resin transfer molding on an MTS 250kN press in a 100x100mm open square mould (see Figure 1). The surface of the mould was cleaned with isopropanol and robbed with Chemlease 2752W from *ChemTrend* to help with the demoulding process. The compression was conducted as follow: (i) the empty mould was closed to set the zero distance, it was then open back to the starting position, (ii) Teflon tape was applied on the junction in the bottom of the mould to avoid any resin leakage, the fibre perform was then set in the mould, (iii) the resin system was poured on top of the fibres and the system was compressed at 0.05 mm/s (last 10mm) until reaching a thickness corresponding to a volume fraction of fibre equal to V_f = 0.4. Note that 1.3x the theoretical amount of resin was used to counterbalance the resin leakage during processing. The plates were then post-cured at 120°C for 2h to finish the cure. The optimization of the cure cycle was performed looking at optical microscopy of polished samples.

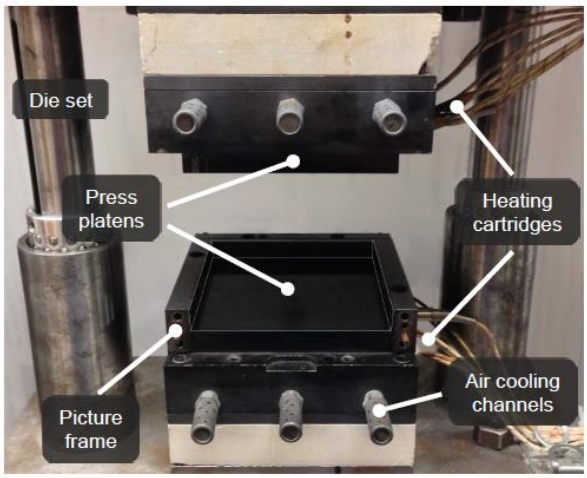

Figure 1: Square mould used for the processing of the plates (the front part was removed for the picture). [9]

Table 1: Details of the fibre nominal superficial density, stack and target thickness for $V_f = 0.4$.

	$\rho_s\ [g/m^2]$	Stack	t_{target} [mm]
Complex	910	$[Mat,90,0]_s$	1.78
Weave	295	$[0,90]_{3s}$	1.73

3 RESULTS & DISCUSSION

Optimization of the moulding cycle and fibres impregnation

The used compression method has several issues when it comes to compression resin transfer moulding. Firstly, the use of an open mould allows for the resin to escape the cavity, the effective moulding pressure is then mostly uncontrolled. Therefore, the moulding cannot be conducted with a control in force but with a control in the final thickness of the plate only. The first tests were conducted with the complex fibres and a mould at 40°C, the pressure profile as well as an optical microscopy of the samples are shown in Figure 3. The pressure profile shows a peak at 0.55 MPa resulting in mostly dry fibre tows, when the space between the tows is adequately filled with resin. In order to increase the effective moulding pressure, a metallic shim was added to create a pinching zone surrounding the fibre bed. The shim was a 3.8 mm thick steal frame with an outer and inner length of 100 and 80mm respectively. This low permeability region should help the resin stay in the mould and help impregnating the fibre tows. The pressure profile as well as an optical microscopy of the samples are shown in Figure 3a and 3c respectively. The first difference with the shim-less configuration (Figure 3b) is the moulding pressure that was increased with the shim to 0.85 MPa. This is resulting in a better impregnation of the fibre tows visible in Figure 3c; however, when some regions are well impregnated, some others are still containing numerous voids. This is a sign that the applied pressure is still too low and/or that the resin is curing too quickly, not letting for the resin to reach the center of each tow before the gel point. A tow impregnation model was used to have an insight of the time required to impregnate the fibre preform [10]:

$$\frac{d\beta}{dt} = \frac{K}{\mu R_{tow}^2 (1 - V_f)} \left(\frac{P_\infty - P_f}{(1-\beta)\ln(1/(1-\beta))} \right) \qquad (1)$$

with β is the degree of impregnation ($0 \leq \beta \leq 1$), R_{tow} is the circular equivalent tow radius, K is the permeability of the preform, μ is the viscosity of the resin system, V_f is the fibre volume fraction in the tow, P_∞ is the applied pressure and P_f is the internal pressure. For simplicity, the capillary pressure contribution was omitted and P_f was considered to the atmospheric pressure, giving a worst-case scenario configuration where the resin doesn't wet the fibres. The increase of viscosity coming from the cure of the resin was also omitted and the tow transverse permeability was estimated from analytical equations proposed by Gebart *et al.* [11], for simplicity. The equivalent fibre tow radius was calculated as follow:

$$R_{tow} = \sqrt{2} \frac{a_0 b_0}{\sqrt{a_0^2 + b_0^2}} \qquad (2)$$

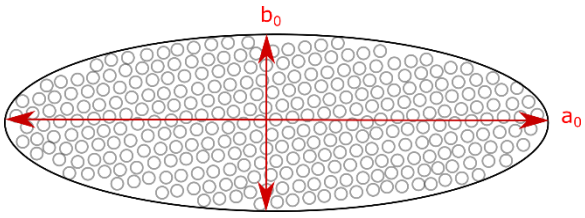

Figure 2: Schematic for the measurement of R_{tow}.

where a_0 and b_0 is the tow width and high respectively (Figure 2).

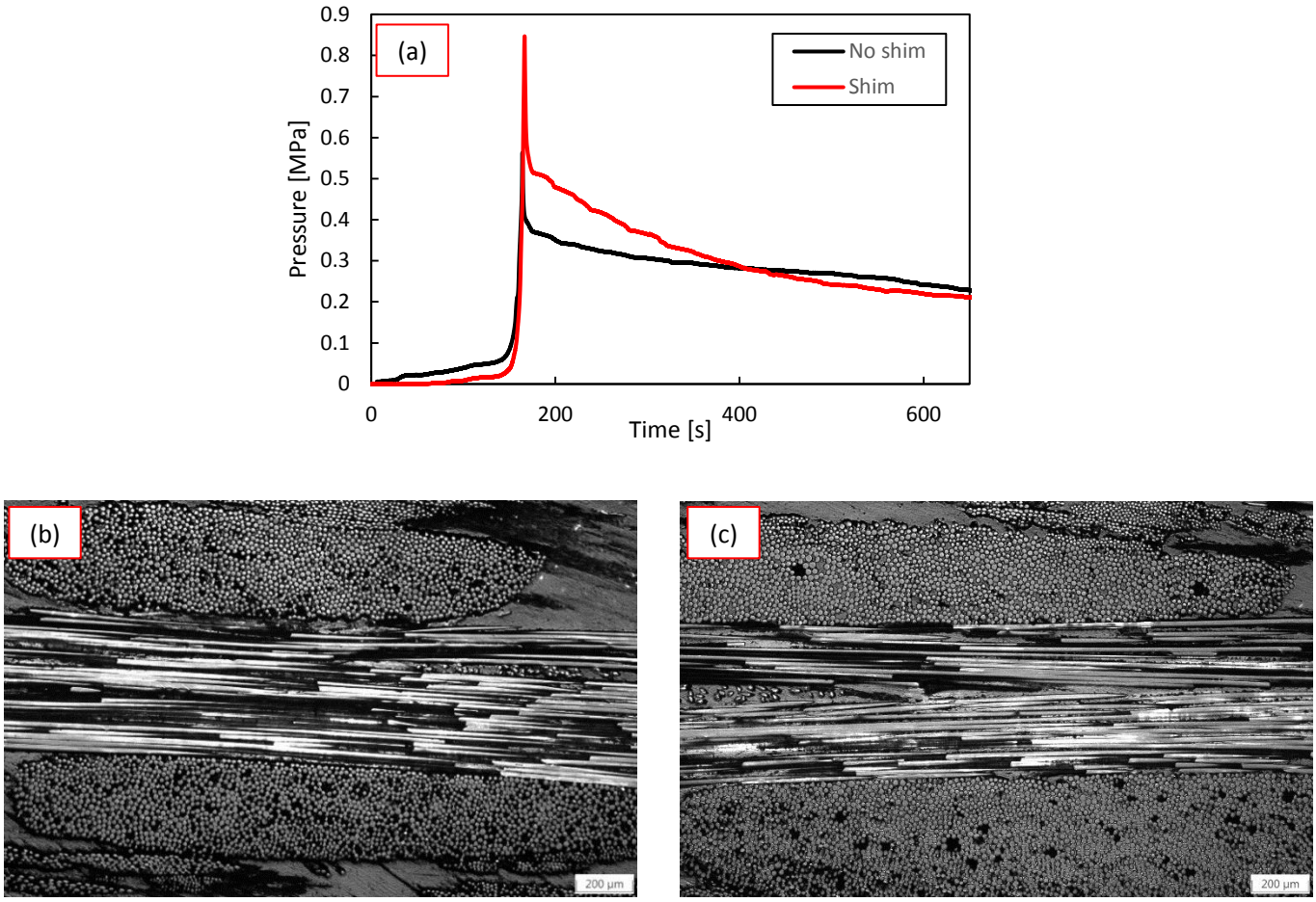

Figure 3: (a) pressure evolution during processing and optical microscopy images of the plate (b) 40°C without shim, (c) 40°C with shim.

The values used in equation (1) are summarized in Table 2, the evolution of the degree of impregnation with time and applied pressure are shown in Figure 4. The system pressed at 0.55 MPa would requires 6 min to be fully impregnated. When this value does not seem excessive, it is dramatic for the resin system studied here that reaches its gel point in approximately 3 min. The compression with the shim at 0.85 MPa would need 3.5 min to be fully impregnated. This value, close to the experimental gel time, is in line with what can be observed in Figure 2c with region fully impregnated (mostly at the top of the plate) and others containing lots of voids (mostly at the bottom of the plate). In such configurations, the applied pressure is then not high enough to have a full impregnation of the fibre. In a second step, the moulding pressure was increased by setting a much higher pressure during the zeroing of the thickness before the moulding (step (i) of the moulding process). Indeed, it was noticed that using a higher pressure during this zeroing step allows to reach high pressure during the moulding step. The same tests were then conducted reaching a pressure of 12MPa (1MPa previously) during the zeroing step. Such pressure would impregnate the fibre tows in a few seconds according to the tow impregnation model (see Figure 4).

Table 2: Parameters used in the tow impregnation model.

$K\ [m^2]$	$1.5 \cdot 10^{-14}$
$R_{tow}\ [m]$	$2.5 \cdot 10^{-4}$
$\mu\ [Pa \cdot s]$	0.17
V_f	0.7
$P_f\ [Pa]$	10^5

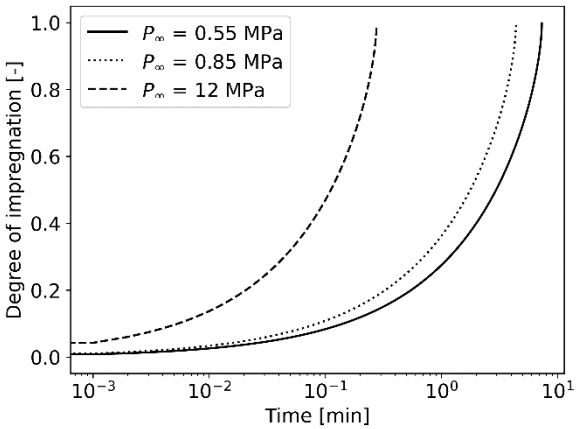

Figure 4: Degree of impregnation as a function of time and applied pressure.

Two temperature cycles were tested, the first one with a hot moulding at 40°C and another one moulding at room temperature leaving the system to "rest" for 15min and then cure the system at 50°C for 10 min. The goal of such comparison was to verify that the quality of the plates cured with a hot mould are equivalents with the "perfect" plates moulded at room temperature. The pressure evolution in each case and optical microscopy images of the samples are shown in Figure 5. The red arrow in Figure 5a shows the bump linked with the start of the cure.

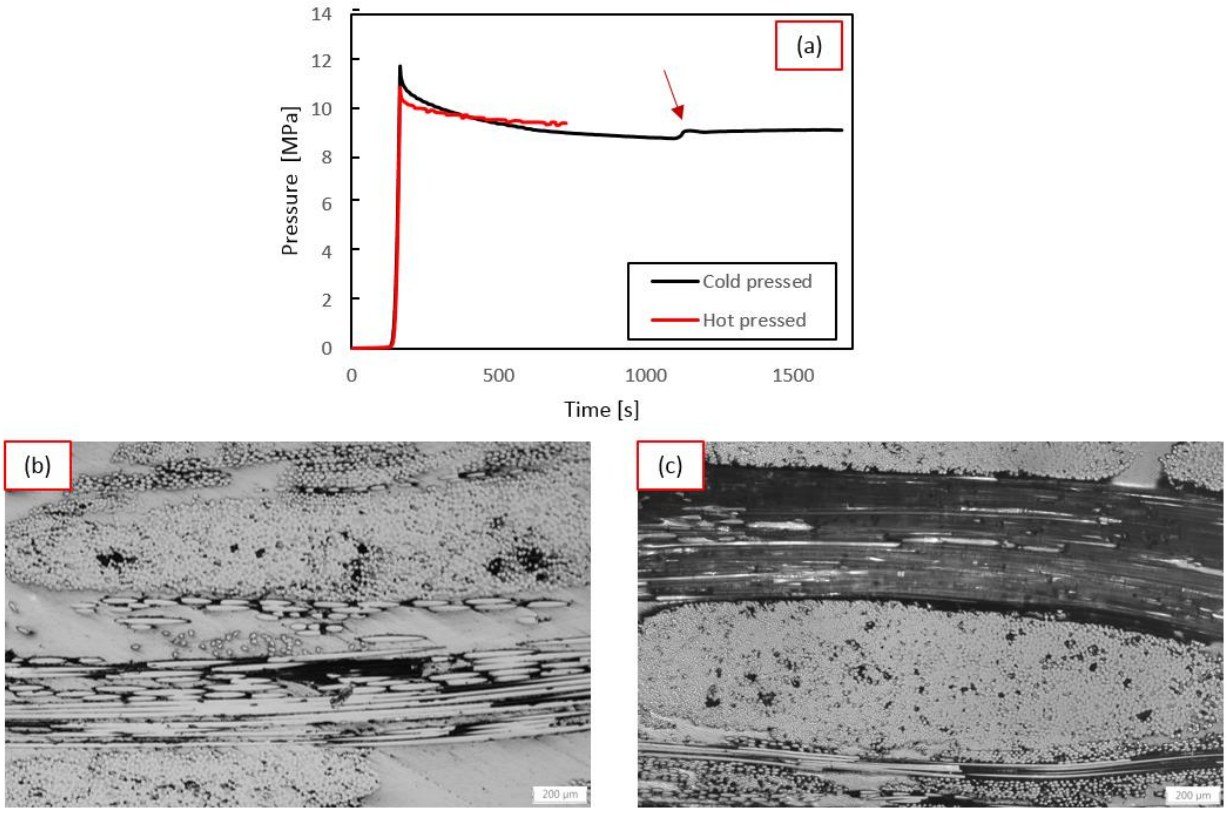

Figure 5: (a) pressure evolution during processing and optical microscopy images of the plate with a zero-thickness at 12MPa (b) cold pressed with shim, (c) 40°C with shim.

Increasing the target load setting the zero thickness indeed increased the moulding pressure. The resulting impregnation is also well improved compared to the lower pressure case shown previously. The center of the tow in each case is well impregnated, following the prediction from the tow impregnation model. Some voids are, however, still observed but they are attributed to the open mould setup where it is difficult to process void free plates. The hot-pressed sample shows a dark transverse fibre tow (see Figure 5c). This most probably comes from the polishing of the sample that pullout out the longitudinal fibres. Both strategies look equivalent and can be used to have a full impregnation of the fibre preform. The cold-pressed strategy was chosen for the rest of the tests because it integrates better into the resin preparation workflow.

Effect on the phase separation

Two possible phenomena could have an influence on the phase separation during the compression process: (i) the increase of pressure affecting the thermodynamic of phase separation (shift of critical point), changing the resulting morphology and (ii) the selective suction of either polymers by the fibre tows that could locally increase/decrease the fraction of thermoplastic in between the tows, as well changing the phase-separated morphology.
To have a better understanding of the effect of fibres on the phase separation, Figure 6 shows the microstructure of a UPE-8wt%PCL blend. The fibre tows are surrounded by the UPE-rich region, the PCL-rich region showing no wetting of the fibre. However, there still PCL-rich region in between the fibres (see Figure 6 red arrow). The repartition of the phase in the fibre tows seems to reflect what was observed in the space in between the tows. There is then no local change in composition effecting the phase separation.

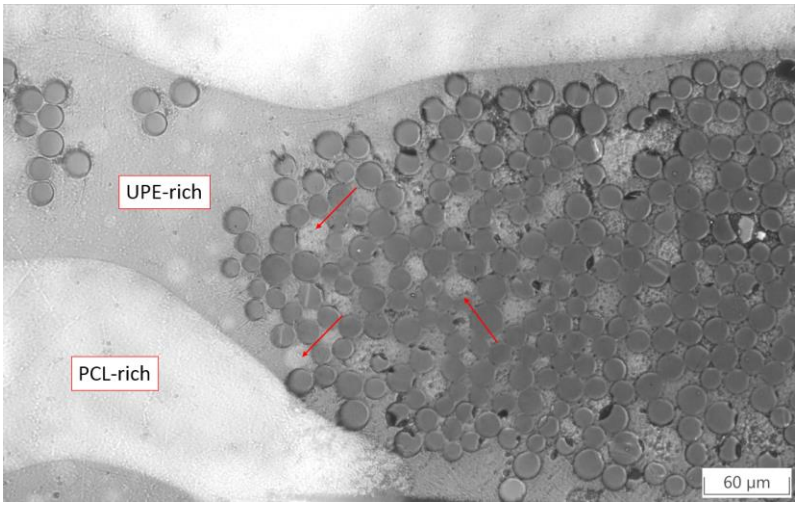

Figure 6: Microscopy image of a UPE-8wt%PCL.

A comparison between two blends with 4 and 7wt%PCL with and without fibres is shown in Figure 7. The phase separated morphology was similar between the systems with and without fibres, confirming that the presence of fibre and the high moulding pressure was not visibly affecting the thermodynamic of phase separation.

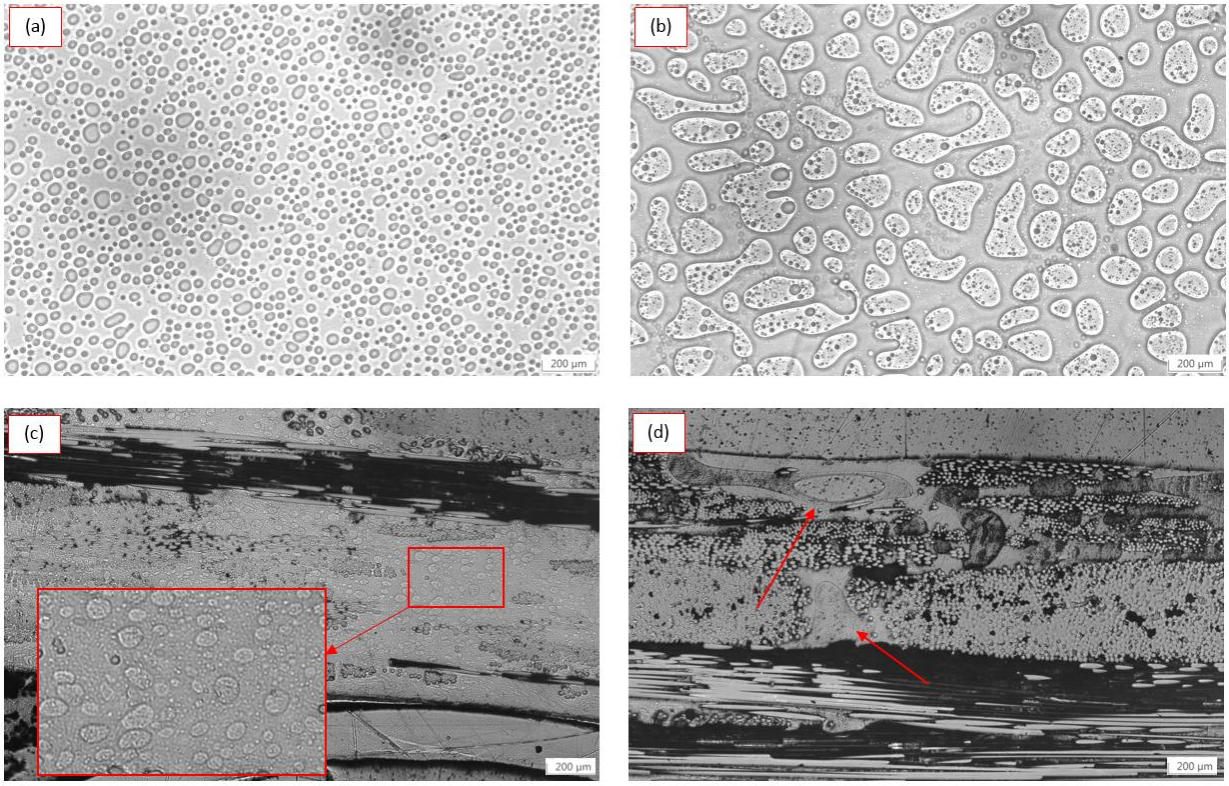

Figure 7: Microscopy images (a) UPE-4wt%PCL without fibres, (b) UPE-7wt%PCL without fibres, (c) UPE-4wt%PCL with fibres, (d) UPE-7wt%PCL with fibres.

Effect of graphene of fibres impregnation and phase separation

The presence of a large quantity of graphene in the resin increases the viscosity of the system and could influence the impregnation of the fibre tows. To study this effect, plates with 8wt% of graphene were produced following the optimized cycle discussed above. An optical microscopy of the polished sample is shown in Figure 8a. Firstly, the impregnation of the fibre tows wasn't affected by the presence of graphene, only few voids being observed in the fibre tows. Secondly, no filtering effect was observed throughout the sample. The graphene forming a continuous path between the fibre tows with only few graphene particles entering the fibre tow. This behaviour was attributed from the non-crimp complex fibre architecture that leaves large channel for the graphene to migrate through the fibre preform. The same test was performed on the weave fibre architecture and is shown Figure 8b. In this case, the graphene particles were completely filtered and left at the surface of the preform. No graphene particles were observed inside the cured preform. There is then a critical distance between the fibre tows to avoid any filtration of particles. A quick image analysis of each system shows an average distance between the tows of $\sim 53 \mu m$ and $\sim 126 \mu m$ for the weave and complex fibre architecture respectively. The average agglomerate size of the graphene powder being close to $30 \mu m$, the distance between the tows for the weave architecture is then too small for the particles to flow freely in the preform. An educated guess would be to have at least three times the average particles size to avoid any filtration effects. In this case, a distance of at least $\sim 90 \mu m$ between the fibre tows would then be necessary to obtain a homogeneous distribution of the graphene through the plate.

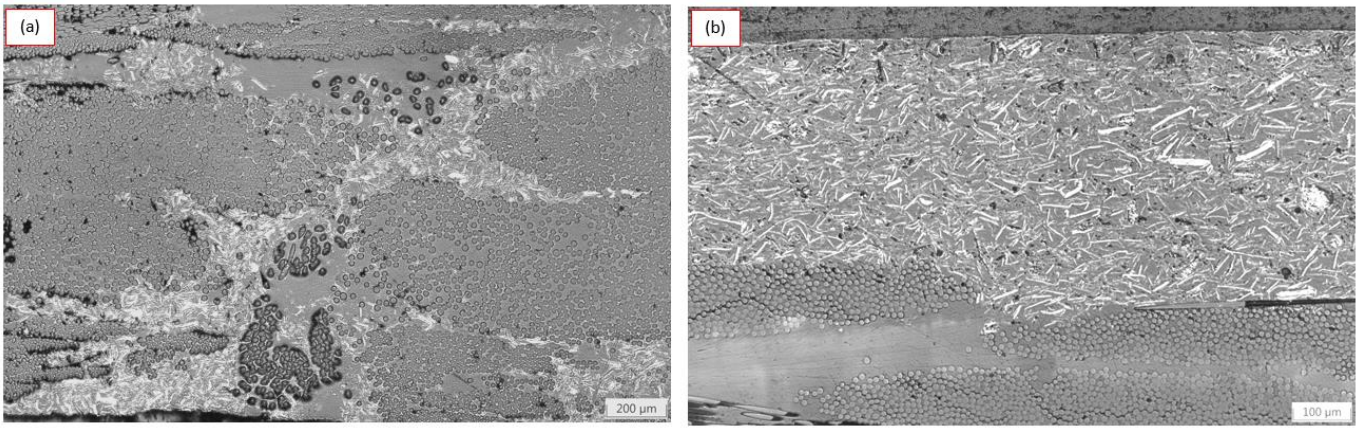

Figure 8: Microscopy images (a) UPE-8wt%gf with the complex fibre architecture (b) UPE-8wt%gf with the weave fibre architecture.

Figure 9 shows a microscopy of a plate with 4wt% off PCL and 8wt% of graphene. When added to a phase separating system, the graphene will stay in the UPE-rich region, leaving the PCL-rich phase totally free of graphene particles. That creates a self-assembly network of graphene rich phase in the matrix. This network could have a positive impact on the fraction of graphene needed to reach the percolation threshold. The phase separated morphology is similar to what was observed in Figure 7c, the addition of graphene has then no substantial effect on the dynamic of phase separation.

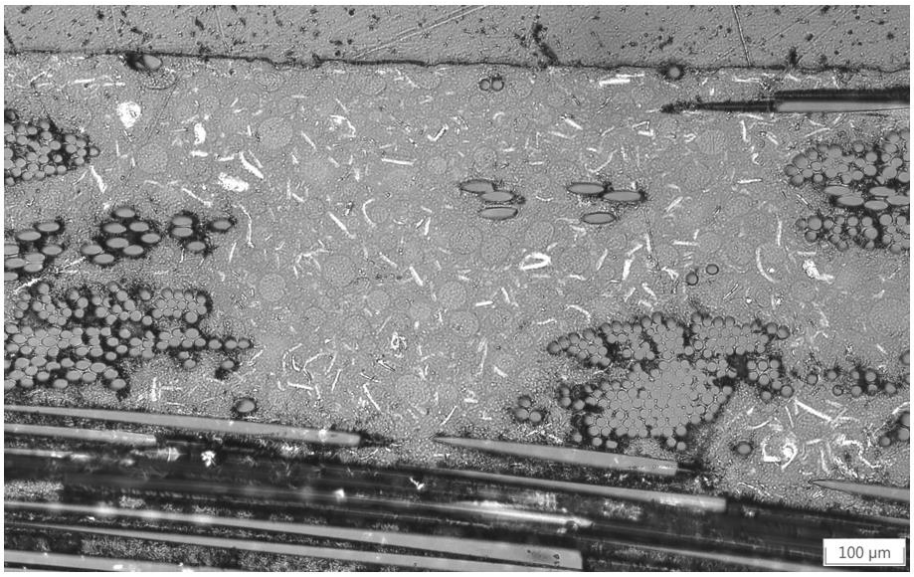

Figure 9: Microscopy image of UPE-4wt%PCL-8wt%gf.

4 CONCLUSION

The impact of the processing parameters on the impregnation of the fibre preform was studied with unsaturated polyester and a complex fibre architecture. The use of an open mould was found to leave the applied pressure too low to have a good impregnation of the fibre bed. A partial solution was to use a metallic shim in order to trap the resin in the mould and increase the effect pressure on the resin. When the resulting part showed some improvements, the quick cure of the resin was the factor limiting for a good impregnation of the fibre tows. A simple tow impregnation model showed that a pressure of 12MPa would infiltrate the fibre tows in a couple seconds. To reach such pressure, the target pressure when setting the zero thickness of the mould was increased to 12MPa. The resulting plates were of required quality, fully impregnated with only a few residual voids. The optimized moulding cycle was tested on phase separating blends and showed no effect on the morphology of phase separation. The obtained morphology being similar to what was observed at low pressure and without fibres. The addition of large quantity of graphene particles to the complex fibre preform showed no filtration effect and resulted on a homogeneous distribution of the particles in between the fibre tows. The same test was conducted on a denser twill weave showing a full filtration of the graphene particles at the surface of the sample. The distance between the fibre tows being too close to the average graphene agglomerates size. The addition of graphene in a blend of unsaturated polyester and polycaprolactone showed a selective localisation of the graphene in the UPE-rich phase leaving the PCL-rich phase totally free of graphene particles. Such composition then creates a self-assembly network of graphene-rich phase reducing the quantity of graphene needed to reach the percolation threshold for electrical conduction. The optimized processing parameters then allows for the production of fully impregnated multiscale multiphase graphene-based composite with promising properties self-sensing properties.

Acknowledgements

The authors would like to thank their funding partners, The Werner Graupe Fellowship, the Natural Sciences and Engineering Research Council of Canada (NSERC) grant RDCPJ 530253-18, Prima Quebec grant R16-46-005, NanoXplore Inc., the Research Center for High Performance Polymer and Composite Systems (CREPEC) and the McGill Engineering Doctoral Awards program (MEDA) for their support.

5 REFERENCES

[1] H. Lui, Q. Li, S. Zhang, R. YIn, X. Liu, Y. He, K. Dai, C. Shan, J. Guo, C. Liu, C. Shen, X. Wang, N. Wang, Z. Wang, R. Wei and Z. Guo, "Electrically conductive polymer composites for smart flexible strain sensors: a critical review," *Journal of Materials Chemistry C,* vol. 6, pp. 12121-12141, 2018.

[2] S. Baril-Gosselin, "INVESTIGATION OF THE RESIN FILM INFUSION PROCESS FOR MULTI-SCALE COMPOSITES BASED ON THE STUDY OF RESIN FLOW, VOID FORMATION AND CARBON NANOTUBE DISTRIBUTION," University of Ottawa, 2018.

[3] Y. Zhang, Y. Shen, K. Shi, T. Wang and E. Harkin-Jones, "Constructing a filler network for thermal conductivty enhancement in epoxy composites via reaction induced phase separation," *Composites Part A,* vol. 110, pp. 62-69, 2018.

[4] I. Sahalianov and O. Lazarenko, "Enhancement of electroconductivity and percolation threshold by the morphology of dielectric network in segregated polymer/ nanocarbon composites," *Materials Research Express,* vol. 6, 2019.

[5] R. Williams, B. Rozenberg and J. Pascault, "Reaction-Induced Phase Separation in Modified Thermosetting Polymers," *Advances in Polymer Science,* vol. 128, pp. 95-156, 1997.

[6] N. Inc., "Technical Data Sheet - GrapheneBlack3X DS-GB 3X-21080, Technical Report," 2021.

[7] A. Bianco, H.-M. Cheng, T. Enoki, Y. Gogosti, R. H. Hurt, N. Koratkar, T. Kyotani, M. Monthioux, C. R. Park, J. M. D. Tascon and J. Zhang, "All in the graphene family - A recommended nomenclature for two-dimensional carbon materials," *Carbon,* vol. I, no. 6, 2013.

[8] P. Wick, A. E. Louw-Gaume, M. Kucki, H. F. Krug, K. Kostarelos, B. Fadeel, K. A. Dawson, A. Salvati, E. Vazquez, L. Ballerini, M. Tretiach, F. Benfenati, E. Flahaut, L. Gauthier, M. Prato and A. Bianco, "Classification Framework for Graphene-Based Materials," *Angewandte Essays,* vol. 53, pp. 7714-7718, 2014.

[9] B. Landry, "Experimental Study and Numerical Simulation of Defect Formation During Compression Moulding of Discontinuous Long Fibre Carbon/PEEK Composites," McGill University, 2015.

[10] T. Centea and P. Hubert, "Modelling the effect of material properties and process parameters on tow impregnation in out-of-autoclave prepregs," *Composites: Part A,* vol. 43, pp. 1505-1513, 2012.

[11] B. R. Gebart, "Permeability of Unidirectional Reinforcements for RTM," *Journal of Composite Materials,* vol. 26, no. 8, pp. 1100-1133, 1992.